PHYSICAL REVIEW D **87,** 082004 (2013)

Template banks to search for low-mass binary black holes in advanced gravitational-wave detectors

Duncan A. Brown, Prayush Kumar, and Alexander H. Nitz

Department of Physics, Syracuse University, Syracuse, New York 13244, USA

(Received 27 November 2012; published 25 April 2013)

Coalescing binary black holes (BBHs) are among the most likely sources for the Laser Interferometer Gravitational-Wave Observatory (LIGO) and its international partners Virgo and KAGRA. Optimal searches for BBHs require accurate waveforms for the signal model and effectual template banks that cover the mass space of interest. We investigate the ability of the second-order post-Newtonian TaylorF2 hexagonal template placement metric to construct an effectual template bank, if the template waveforms used are effective one-body waveforms tuned to numerical relativity (EOBNRv2). We find that by combining the existing TaylorF2 placement metric with EOBNRv2 waveforms, we can construct an effectual search for BBHs with component masses in the range $3M_\odot \leq m_1, m_2 \leq 25M_\odot$. We also show that the (computationally less expensive) TaylorF2 post-Newtonian waveforms can be used in place of EOBNRv2 waveforms when $M \lesssim 11.4M_\odot$. Finally, we investigate the effect of modes other than the dominant $l = m = 2$ mode in BBH searches. We find that for systems with $(m_1/m_2) \leq 1.68$ or inclination angle $\iota \leq 0.31$ or $\iota \geq 2.68$ radians, there is no significant loss in the total possible signal-to-noise ratio due to neglecting modes other than $l = m = 2$ in the template waveforms. For a source population uniformly distributed in spacial volume, over the entire sampled region of the component-mass space, the loss in detection rate (averaged over a uniform distribution of inclination angle and sky-location/polarization angles) remains below ~11%. For binaries with high mass ratios *and* $0.31 \leq \iota \leq 2.68$, including higher-order modes could increase the signal-to-noise ratio by as much as 8% in Advanced LIGO. Our results can be used to construct matched-filter searches in Advanced LIGO and Advanced Virgo.

DOI: 10.1103/PhysRevD.87.082004 PACS numbers: 04.80.Nn, 04.25.Nx, 04.30.Db

I. INTRODUCTION

Over the last decade, there has been tremendous progress towards the first direct detection of gravitational waves. Construction of the Advanced Laser Interferometer Gravitational-Wave Observatory (aLIGO) is underway, with completion scheduled for 2014 [1]. Similar upgrades to the French-Italian Virgo detector [2] have commenced and construction of the Japanese KAGRA detector has begun [3]. When these second-generation gravitational-wave detectors reach design sensitivity, they will increase the observable volume of the universe by a thousandfold or more [4], compared to the first-generation detectors.

The inspiral and merger of binary black holes (BBHs) are expected to be an important source for detection by aLIGO [5]. The rate of BBH coalescences that will be observed by aLIGO at design sensitivity is estimated to be between 0.2 yr^{-1} and 1000 yr^{-1} [6]. Accurate knowledge of the gravitational-wave signals generated by BBHs is crucial for detecting and extracting information about these sources. To provide such waveforms, the effective one-body (EOB) model [7] has been calibrated to numerical simulations of black hole (BH) mergers [8–15]. A new EOB waveform family (called EOBNRv2) has been recently proposed that incorporates information from several nonspinning BBH simulations, with black hole ring-down quasinormal modes [16,17] attached to provide a complete BBH waveform [15]. The EOBNRv2 waveform is believed to be sufficiently accurate to search for nonspinning BBH signals in the aLIGO sensitive band (10–1000 Hz).

Past searches for BBHs [18–22] used matched filtering [23,24] to search for coalescing compact binaries. These searches divided the BBH mass space into a *low-mass* region with $M = m_1 + m_2 \lesssim 25M_\odot$ and a *high-mass* region with $M \gtrsim 25M_\odot$. In this paper, we focus attention on BBH systems with component masses between $3M_\odot \lesssim m_1, m_2 \lesssim 25M_\odot$, which encompasses the mass distribution of black hole candidates observed in low-mass X-ray binaries [25]. aLIGO will be able to detect coalescing BBH systems with component masses $m_1 = m_2 = 25M_\odot$ to a maximum distance of up to ~3.6 Gpc. Since we do not know *a priori* the masses of BBHs that gravitational-wave detectors will observe, searches use a *bank* of template waveforms which covers the range of BBH component masses of interest [26,27]. This technique is sensitive to the accuracy of the waveform templates that are used as filters and the algorithm used to place the template waveforms [28]. An accurate template bank is required as input for matched filter searches in the Fourier domain [24], as well as newer search algorithms such as the singular value decomposition [29].

In this paper, we investigate three items of importance to advanced-detector BBH searches. First, we study the accuracy of template placement algorithms for BBH searches

using EOBNRv2 waveforms. Optimal template placement requires a metric for creating a grid of waveforms in the desired region of parameter space [30]; however, no analytic metric exists for the EOBNRv2 waveform. In the absence of such a metric, we construct a template bank using the second-order post-Newtonian hexagonal placement algorithm [31–34]. This metric is used to place template grid points for the aLIGO zero-detuning high-power sensitivity curve [35] and we use EOBNRv2 waveforms at these points as search templates. We find that the existing algorithm works well for BBHs with component masses in the range $3M_\odot \leq m_1, m_2 \leq 25M_\odot$. For a template bank constructed with a minimal match of 97% less than 1.5% of nonspinning BBH signals have a mismatch greater than 3%. We therefore conclude that the existing bank placement algorithm is sufficiently accurate for nonspinning BBH searches in this mass region. Second, we investigate the mass range in which the (computationally less expensive) third-and-a-half-order TaylorF2 post-Newtonian waveforms [26,36–44] can be used without significant loss in event rate, and where full inspiral-merger-ring-down EOBNRv2 waveforms are required. We construct a TaylorF2 template bank designed to lose no more than 3% of the matched filter signal-to-noise ratio and use the EOBNRv2 model as signal waveforms. We find that for nonspinning BBHs with $M \lesssim 11.4M_\odot$, the TaylorF2 search performs as expected, with a loss of no more than 10% in the event rate. For higher masses larger event rate losses are observed. A similar study was performed in Ref. [45] using an older version of the EOB model and our results are quantitatively similar. We therefore recommend that this limit be used as the boundary between TaylorF2 and EOBNRv2 waveforms in Advanced LIGO searches. Finally, we investigate the effect of modes other than the dominant $l = m = 2$ mode on BBH searches in aLIGO. The horizion distance of aLIGO (and hence the event rate) is computed considering only the dominant mode of the emitted gravitational waves, since current searches only filter for this mode [6]. However, the inclusion of sub-dominant modes in a gravitational-wave template could increase the reach of aLIGO [46,47]. If we assume that BBH signals are accurately modeled by the EOBNRv2 waveform including the five leading modes, we find that for systems with $(m_1/m_2) \leq 1.68$ or inclination angle $\iota \geq 2.68$ or $\iota \leq 0.31$ radians, there is no significant loss in the total possible signal-to-noise ratio due to neglecting modes other than $l = m = 2$ in the template waveforms, if one uses a 97% minimal-match bank placed using the hexagonal bank placement algorithm [31–34]. However, for systems with mass ratio $(q) \geq 4$ and $1.08 \leq \iota \leq 2.02$, including higher-order modes could increase the signal-to-noise ratio by as much as 8% in aLIGO. This increase in amplitude may be offset by the increase in the false-alarm rate from implementing searches which also include sub-dominant waveform modes in templates, so we encourage the investigation of such algorithms in real detector data.

The remainder of this paper is organized as follows. In Sec. II we review the gravitational waveform models used in this study. In Sec. III we present the results of large-scale Monte Carlo signal injections to test the effectualness of the template banks under investigation. Finally, in Sec. IV we review our findings and recommendations for future work.

II. WAVEFORMS AND TEMPLATE BANK PLACEMENT

A. Waveform approximants

The dynamics of a BBH system can be broadly divided into three regimes. (i) The early inspiral, when the separation between the black holes is large and their velocity is small, can be modeled using results from post-Newtonian (PN) theory [48]. The gravitational-wave phasing of nonspinning binaries is available up to 3.5PN order [38–44]. (ii) Accurately modeling the late inspiral and merger requires the numerical solution of the Einstein equations [49–55]. (iii) The final ring-down phase can be modeled using a superposition of quasinormal modes (QNMs) which describe the oscillations of the perturbed Kerr black hole that is formed from the coalescence [16,17].

Numerical simulations of BBH systems are computationally expensive, and results are only available for a relatively small number of binary systems (see, e.g., Ref. [56]). The EOB model [7] provides a framework for computing the gravitational waveforms emitted during the inspiral and merger of BBH systems. By attaching a QNM waveform and calibrating the model to numerical relativity (NR) simulations, the EOB framework provides for accurate modeling of complete BBH waveforms (EOBNR). The EOBNR waveforms can be computed at relatively low cost for arbitrary points in the waveform parameter space [8–15]. In particular, the EOB model has recently been tuned against high-accuracy numerical relativity simulations of nonspinning BBHs of mass ratios $q = \{1, 2, 3, 4, 6\}$, where $q \equiv m_1/m_2$ [15]; we refer to this as the EOBNRv2 model, which we review the major features of below. Throughout, we set $G = c = 1$.

The EOB approach maps the fully general-relativistic dynamics of the two-body system to that of an *effective* mass moving in a deformed Schwarzschild spacetime [7]. The physical dynamics is contained in the deformed spacetime's metric coefficients, the EOB Hamiltonian [7], and the radiation-reaction force. In polar coordinates (r, Φ), the EOB metric is written as

$$ds^2_{\rm eff} = -A(r)dt^2 + \frac{A(r)}{D(r)}dr^2 + r^2(d\Theta^2 + \sin^2\Theta d\Phi^2). \quad (1)$$

The geodesic dynamics of the *effective* mass $\mu = m_1m_2/M$ in the background of Eq. (1) is described by an

effective Hamiltonian $H^{\rm eff}$ [7,57]. The EOBNRv2 model uses Pade resummations of the third-order post-Newtonian Taylor expansions of the metric coefficients $A(r)$ and $D(r)$, with additional 4PN and 5PN coefficients that are calibrated [9–12,15] to ensure that the dynamics agrees closely with NR simulations of comparable mass binaries.

Gravitational waves carry energy and angular momentum away from the binary, and the resulting radiation-reaction force $\hat{F}_\Phi$ causes the orbits to shrink. This is related to the energy flux as

$$\hat{F}_\Phi = -\frac{1}{\eta\hat{\Omega}}\frac{dE}{dt} = -\frac{1}{\eta v^3}\frac{dE}{dt}, \tag{2}$$

where $v = (\hat{\Omega})^{1/3} = (\pi M f)^{1/3}$ and f is the instantaneous gravitational-wave frequency. The energy flux dE/dt is obtained by summing over the contribution from each term in the multipole expansion of the waveform, i.e.,

$$\frac{dE}{dt} = \frac{\hat{\Omega}^2}{8\pi}\sum_l\sum_m \left|\frac{\mathcal{R}}{M}h_{lm}\right|^2. \tag{3}$$

$\mathcal{R}$ is the physical distance to the binary and h_{lm} are the multipoles of the waveform when it is decomposed in a spin-weighted spherical harmonic basis as

$$h_+ - ih_\times = \frac{M}{\mathcal{R}}\sum_{l=2}^{\infty}\sum_{m=-l}^{m=l} Y^{lm}_{-2}h_{lm}, \tag{4}$$

where Y^{lm}_{-2} are the spin-weighted spherical harmonics, and h_+ and $h_\times$ are the two orthogonal gravitational-wave polarizations. These waveform multipoles depend on the coordinates and their conjugate momenta, and their Taylor expansions were resummed as products of individually resummed factors [58],

$$h_{lm} = h^F_{lm}N_{lm}, \tag{5a}$$

$$h^F_{lm} = h^{(N,\epsilon)}_{lm}\hat{S}^{(\epsilon)}_{\rm eff}T_{lm}e^{i\delta_{lm}}(\rho_{lm})^l, \tag{5b}$$

where ϵ is 0 if $(l+m)$ is even, and is 1 otherwise. This factorized resummation of the waveform multipoles ensures agreement with NR waveform multipoles [8–10]. The first factor $h^{(N,\epsilon)}_{lm}$ is the resummation of the Newtonian-order contribution and the second factor $\hat{S}^{(\epsilon)}_{\rm eff}$ is the source term, given by the mass or the current moments of the binary in the EOB formalism [58,59]. The tail term T_{lm} is the resummation of the leading-order logarithmic terms that enter into the transfer function of the near-zone multipolar waves to the far-zone ones [59]. The last term N_{lm} attempts to capture the noncircularity of the quasicircular orbits. While calculating the energy flux in this study we follow exactly the prescription of Ref. [15], which calibrates the coefficients of the flux so that resulting EOB waveform multipoles reproduce their NR counterparts with high accuracy.

We use the EOBNRv2 Hamiltonian and flux in the equations of motion for the binary, given by

$$\frac{dr}{d\hat{t}} \equiv \frac{\partial\hat{H}^{\rm real}}{\partial p_r} = \frac{A(r)}{\sqrt{D(r)}}\frac{\partial\hat{H}^{\rm real}}{\partial p_{r*}}(r, p_{r*}, p_\Phi), \tag{6a}$$

$$\frac{d\Phi}{d\hat{t}} \equiv \hat{\Omega} = \frac{\partial\hat{H}^{\rm real}}{\partial p_\Phi}(r, p_{r*}, p_\Phi), \tag{6b}$$

$$\frac{dp_{r_*}}{d\hat{t}} = -\frac{A(r)}{\sqrt{D(r)}}\frac{\partial\hat{H}^{\rm real}}{\partial r}(r, p_{r*}, p_\Phi), \tag{6c}$$

$$\frac{dp_\Phi}{d\hat{t}} = \hat{F}_\Phi(r, p_{r*}, p_\Phi), \tag{6d}$$

where $\hat{t}(\equiv t/M)$ is time in dimensionless units.

To obtain the initial values of the coordinates $(r, \Phi, p_{r_*}, p_\Phi)$ that the system starts out in, we use the conditions for motion on spherical orbits derived in Ref. [60], where they treated the case of a generic precessing binary. We take their nonspinning limit to define the initial configuration of the binary, requiring

$$\frac{\partial\hat{H}^{\rm real}}{\partial r} = 0, \tag{7a}$$

$$\frac{\partial\hat{H}^{\rm real}}{\partial p_{r_*}} = \frac{1}{\eta}\frac{dE}{dt}\frac{(\partial^2\hat{H}^{\rm real}/\partial r\partial p_\Phi)}{(\partial\hat{H}^{\rm real}/\partial p_\Phi)(\partial^2\hat{H}^{\rm real}/\partial r^2)}, \tag{7b}$$

$$\frac{\partial\hat{H}^{\rm real}}{\partial p_\Phi} = \hat{\Omega}_0, \tag{7c}$$

where $\hat{\Omega}_0 = \pi M f_0$, with f_0 being the starting gravitational-wave frequency. Simplifying Eq. (7a), and ignoring the terms involving p_{r_*}, as $p_{r_*} \ll p_\Phi/r$ in the early inspiral, we get a relation between p_Φ and r,

$$p^2_\Phi = \frac{r^3A'(r)}{2A(r) - rA'(r)}, \tag{8}$$

where the prime($'$) denotes $\partial/\partial r$. Substituting this into Eq. (7c), we get the relation,

$$\frac{A'(r)}{2r\left(1 + 2\eta\left(\frac{A(r)}{\sqrt{A(r)-\frac{1}{2}rA'(r)}} - 1\right)\right)} = \hat{\Omega}^2_0. \tag{9}$$

Thus, between Eqs. (9) and (8), we get the initial values of (r, p_Φ), corresponding to the initial gravitational-wave frequency f_0, and by substituting these into Eq. (7b), we obtain the initial value of p_{r_*}. With these values, we integrate the equations of motion to obtain the evolution of the coordinates and momenta $[r(t), \Phi(t), p_r(t), p_\Phi(t)]$ over the course of the inspiral, until the light ring is reached. In the EOB model, the light ring is defined as the local maximum of the orbital frequency $\hat{\Omega}$. From the coordinate evolution, we also calculate $h^F_{lm}(t)$, which is the analytic expression for the waveform multipole without the non-quasicircular correction factor [defined in Eq. (5b)]. While generating $h^F_{lm}(t)$ from the dynamics, the values for the free parameters in the expressions for δ_{lm} and ρ_{lm} are taken from Eqs. [38a–39b] of Ref. [15], where they optimize these parameters to minimize the phase and amplitude discrepancy between the respective EOB waveform multipoles and those extracted from NR simulations.

The EOB ring-down waveform is modeled as a sum of N quasinormal modes [9,10,12,16],

$$h^{\mathrm{RD}}_{lm}(t) = \sum_{n=0}^{N-1} A_{lmn} e^{-\mathrm{i}\sigma_{lmn}(t-t^{\mathrm{match}}_{lm})}, \tag{10}$$

where $N = 8$ for the model we consider. The matching time t^{match}_{lm} is the time at which the inspiral-plunge and the ring-down waveforms are attached and is chosen to be the time at which the amplitude of the inspiral-plunge part of $h_{lm}(t)$ peaks (i.e., t^{lm}_{peak}) [9,15]. The complex frequencies of the modes σ_{lmn} depend on the mass M_f and spin a_f of the black hole (BH) that is formed from the coalescence of the binary. We use the relations of Ref. [15], given by

$$\frac{M_f}{M} = 1 + \left(\sqrt{\frac{8}{9}} - 1\right)\eta - 0.4333\,\eta^2 - 0.4392\,\eta^3, \tag{11a}$$

$$\frac{a_f}{M} = \sqrt{12}\,\eta - 3.871\,\eta^2 + 4.028\,\eta^3. \tag{11b}$$

Using the mass and spin of the final BH, the complex frequencies of the QNMs can be obtained from Ref. [16], where these were calculated using perturbation theory. The complex amplitudes A_{lmn} are determined by a hybrid-comb numerical matching procedure described in detail in Sec. II C of Ref. [15].

Finally, we combine the inspiral waveform multipole $h_{lm}(t)$ and the ring-down waveform $h^{\mathrm{RD}}(t)$ to obtain the complete inspiral-merger-ring-down EOB waveform $h^{\mathrm{IMR}}(t)$,

$$h^{\mathrm{IMR}}_{lm}(t) = h_{lm}(t)\Theta(t^{\mathrm{match}}_{lm} - t) + h^{\mathrm{RD}}(t)\Theta(t - t^{\mathrm{match}}_{lm}), \tag{12}$$

where $\Theta(x) = 1$ for $x \geq 0$, and 0 otherwise. These multipoles are combined to give the two orthogonal polarizations of the gravitational waveform, h_+ and $h_\times$,

$$h_+ - \mathrm{i}h_\times = \frac{M}{\mathcal{R}} \sum_l \sum_m Y^{lm}_{-2}(\iota, \theta_c) h^{\mathrm{IMR}}_{lm}, \tag{13}$$

where ι is the inclination angle that the binary's angular momentum makes with the line of sight, and θ_c is a fiduciary phase angle. To ensure the correctness of our results, we wrote independent code to implement the EOBNRv2 waveform based solely on the content of Ref. [15]. We then validated our code against the EOBNRv2 waveform algorithm in the LSC Algorithm Library (LAL) [61]. We find agreement between these two implementations, giving us confidence in both our results and the correctness of the LAL EOBNRv2 code.

Previous searches for stellar-mass BBHs with total mass $M \lesssim 25 M_\odot$ in LIGO and Virgo used the restricted TaylorF2 PN waveforms [26,36,37]. Since this waveform is analytically generated in the frequency domain, it has two computational advantages over the EOBNRv2 model. First, the TaylorF2 model does not require either the numerical solution of coupled ODEs or a Fourier transform to generate the frequency-domain signal required by a matched filter. We compared the speed of generating and Fourier-transforming EOBNRv2 waveforms to the speed of generating Taylor F2 waveforms in the frequency domain, and found that the former can be $\mathcal{O}(10^2)$ times slower than the latter. Second, the TaylorF2 model can be implemented trivially as a kernel on graphics processing units (GPU), allowing search pipelines to leverage significant speed increases due to the fast floating-point performance of GPU hardware. We found the generation of TaylorF2 waveforms using GPUs to be $\mathcal{O}(10^4)$ times faster than generating and Fourier-transforming EOBNRv2 waveforms on CPUs. However, the use of the TaylorF2 waveform may result in a loss in search efficiency due to inaccuracies of the PN approximation for BBHs. To investigate the loss in search efficiency versus computational efficiency, we use the restricted TaylorF2 waveform described below.

The Fourier transform of a gravitational waveform $h(t)$ is defined by

$$\tilde{h}(f) = \int_{-\infty}^{\infty} e^{-2\pi \mathrm{i} f t} h(t) \mathrm{d}t. \tag{14}$$

Using the stationary phase approximation [62], the Taylor F2 waveform $\tilde{h}(f)$ can be written directly in the frequency domain as

$$\tilde{h}(f) = A f^{-7/6} e^{\mathrm{i}\Psi(f)}, \tag{15}$$

where we have kept only the leading-order amplitude terms; this is known as the restricted PN waveform. The amplitude $A \propto \mathcal{M}_c^{5/6}/\mathcal{R}$, where $\mathcal{M}_c$ is the *chirp mass* of the binary, $\mathcal{M}_c = (m_1 + m_2)\eta^{3/5}$, $\eta = m_1 m_2/(m_1 + m_2)^2$ is the symmetric mass ratio, and $\mathcal{R}$ is the distance to the binary. The Fourier phase of the waveform at 3.5PN order is given by [24,26,36,63–66]

$$\begin{aligned}\Psi(f) = {} & 2\pi f t_c - \phi_c - \frac{\pi}{4} + \frac{3}{128}\frac{1}{\eta} v^{-5}\Bigg[1 + \left(\frac{3715}{756} + \frac{55}{9}\eta\right)v^2 - 16\pi v^3 + \left(\frac{15293365}{508032} + \frac{27145}{504}\eta + \frac{3085}{72}\eta^2\right)v^4 \\ & + \left(\frac{38645}{756} - \frac{65}{9}\eta\right)\left(1 + 3\log\left(\frac{v}{v_{\mathrm{lso}}}\right)\right)\pi v^5 + \Bigg[\frac{11583231236531}{4694215680} - \frac{640}{3}\pi^2 - \frac{6848}{21}\gamma_E - \frac{6828}{21}\log(4v) \\ & + \left(-\frac{15737765635}{3048192} + \frac{2255}{12}\pi^2\right)\eta + \frac{76055}{1728}\eta^2 - \frac{127825}{1296}\eta^3\Bigg]v^6 + \left(\frac{77096675}{254016} + \frac{378515}{1512}\eta - \frac{74045}{756}\eta^2\right)\pi v^7\Bigg],\end{aligned} \tag{16}$$

where $v = (\pi M f)^{1/3}$ is the characteristic velocity of the binary, and γ is Euler's constant. The initial conditions are set by starting the waveform from a given gravitational-wave frequency $f = f_{\rm low}$, and the waveform is terminated at the frequency of a test particle at the innermost stable circular orbit of a Schwarzschild black hole ($r = 6M$).

B. Bank placement metric

The noise-weighted overlap between two waveforms h_1 and h_2 can be written as

$$(h_1|h_2) \equiv 2\int_{f_{\rm min}}^{f_{\rm max}} \frac{\tilde{h}_1^*(f)\tilde{h}_2(f) + \tilde{h}_1(f)\tilde{h}_2^*(f)}{S_n(f)}\,{\rm d}f, \qquad (17)$$

where $S_n(f)$ is the one-sided power spectral density of the detector noise. The normalized overlap between the two waveforms is given by

$$(\hat{h}_1|\hat{h}_2) = \frac{(h_1|h_2)}{\sqrt{(h_1|h_1)(h_2|h_2)}}. \qquad (18)$$

In addition to the two mass parameters of the binary, this normalized overlap is also sensitive to the relative phase of coalescence ϕ_c and to the difference in the time of coalescence between the two waveforms h_1 and h_2, t_c. These two parameters (ϕ_c, t_c) can be analytically maximized over to get the maximized overlap $\mathcal{O}$,

$$\mathcal{O}(h_1, h_2) = \max_{\phi_c, t_c} (\hat{h}_1|\hat{h}_2 e^{{\rm i}(2\pi f t_c - \phi_c)}), \qquad (19)$$

which gives a measure of how "close" the two waveforms are in the waveform manifold. The mismatch M between the same two waveforms is written as

$$M(h_1, h_2) = 1 - \mathcal{O}(h_1, h_2). \qquad (20)$$

The match [Eq. (19)] can be regarded as an inner product on the space of intrinsic template parameters, and thus one can define a *metric* on this space [30,33] (at the point θ_1) as

$$g_{ij}(\theta_1) = -\frac{1}{2}\frac{\partial^2 \mathcal{O}(h(\theta_1), h(\theta_2))}{\partial {\theta_1}^i \partial {\theta_2}^j}\bigg|_{\theta_1^k = \theta_2^k}, \qquad (21)$$

where θ_1 is the set of intrinsic parameters (i.e., m_1, m_2 or some combination) of the binary. Thus the mismatch between waveforms produced by systems with nearly equal mass parameters can be given by

$$M(h(\theta), h(\theta + \Delta\theta)) \simeq g_{ij}(\theta)\Delta\theta^i \Delta\theta^j. \qquad (22)$$

For the TaylorF2 approximant, $h(\theta)$ is given by Eqs. (15) and (16), and hence by using Eqs. (17) and (19) we can get $\mathcal{O}(h(\theta_1), h(\theta_2))$ as an analytic function of θ_1 and θ_2 (albeit involving an integral over frequency). This gives a measure of mismatches between neighboring points in the manifold of the mass parameters, and hence a hexagonal two-dimensional lattice placement can be used in the manifold of the mass parameters (see Ref. [33] and references therein) to construct a geometric lattice-based template bank [30,31,33].

On the other hand, for the EOBNRv2 approximant, $h(\theta)$ is obtained through numerical solutions of the Hamiltonian equations, Eq. (6). In this case, the calculation of the metric would involve derivatives of coordinate evolution obtained from numerically integrated equations of motion, which could introduce numerical instabilities in the metric. So the concept of a metric, as in Eq. (21), cannot be used in a convenient (semi)analytic form for the construction of a bank with the EOBNRv2 approximant.

III. RESULTS

To assess the effectualness of the template banks constructed here, we compute the fitting factors [28] of the template bank, defined as follows. If h_a^e is the waveform emitted by a BBH system, then the *fitting factor* of a bank of template waveforms (modeled using approximant X) for this waveform is defined as the maximum value of maximized normalized overlaps between h_a^e and all members $h_b^{\rm X}$ of the bank of template waveforms [28], i.e.,

$$\mathcal{FF}(a, {\rm X}) = \max_{b \in {\rm bank}} \mathcal{O}(h_a^e, h_b^{\rm X}). \qquad (23)$$

This quantity simultaneously quantifies the loss in recovered signal-to-noise ratio (SNR) due to the discreteness of the bank, and the inaccuracy of the template model. The similarly defined quantity MM (minimal match) quantifies the loss in SNR due to only the discreteness of the bank as both the *exact* and the template waveform is modeled with the same waveform model, i.e.,

$${\rm MM} = \min_a \max_{b \in {\rm bank}} \mathcal{O}(h_a^{\rm X}, h_b^{\rm X}), \qquad (24)$$

where a is any point in the space covered by the bank, and X is the waveform approximant. For a detection search that aims at less than 10%(15%) loss in the event detection rate due to the discreteness of the bank and the inaccuracy of the waveform model, we require a bank of template waveforms that has $\mathcal{FF}$ above 0.965 (0.947) [45,67,68]. Throughout, we use the aLIGO zero-detuning high-power noise curve as the power spectral density for bank placement and overlap calculations, and set $f_{\rm min} = 15$ Hz. The waveforms are generated at a sample rate of 8192 Hz, and we set $f_{\rm max} = 4096$ Hz, i.e., the Nyquist frequency.

The expectation value of the SNR for a signal, ρ, from a source located at a distance D is proportional to $1/D$, which comes from the dependence of the amplitude on the distance. In other words, the range to which a source can be seen by the detector

$$D_{\rm obs} = \frac{(g, g)}{\rho^*}, \qquad (25)$$

where g is the gravitational-wave strain produced by the same source at the detector, when located at a unit distance from the detector, and ρ^* is the threshold on SNR required

for detection (typically taken as $\rho^* = 8$). For nonprecessing binaries, for which the sky-location (θ, ϕ) and polarization angles (ψ) do not change over the course of inspiral, the effective volume in which the same source can be detected is $\propto D^3_{\rm obs}$ [69], i.e.,

$$\mathrm{V}_{\rm obs} = kD^3_{\rm obs}, \tag{26}$$

where the proportionality constant k comes from averaging over various possible sky positions of the binary. The use of discrete template banks, and lack of knowledge of the *true* gravitational-wave signal model, leads to the observed SNR ρ' being lower than the optimal SNR $\rho = (h, h)$, i.e.,

$$\rho' = \mathcal{FF}\rho, \tag{27}$$

where $\mathcal{FF}$ is the fitting factor of the template bank employed in the search for the particular system. The observable volume hence goes down as

$$\mathrm{V}^{\rm eff}_{\rm obs} = k(\mathcal{FF} \times D_{\rm obs})^3. \tag{28}$$

If we assume that the source population is distributed uniformly in spacial volume in the universe, then the ratio $\mathrm{V}^{\rm eff}_{\rm obs}/\mathrm{V}_{\rm obs}$ also gives the fraction of systems within the detector's reach that will be seen by the matched-filtering search. For a system with given mass parameters θ_1, the ratio of the total $\mathrm{V}^{\rm eff}_{\rm obs}$ available to it for different inclinations and sky locations to the total $\mathrm{V}_{\rm obs}$ available to it for the same samples of angles will give an estimate of the fraction of systems with those masses (marginalized over other parameters—they being uniformly distributed) that will be seen by the matched-filter search. We refer to this quantity,

$$\epsilon_{\rm V}(\theta_1) = \frac{\sum_{\theta_2} \mathrm{V}^{\rm eff}_{\rm obs}(\theta_1, \theta_2)}{\sum_{\theta_2} \mathrm{V}_{\rm obs}(\theta_1, \theta_2)}, \quad = \frac{\sum_{\theta_2} \mathcal{FF}^3(\theta_1, \theta_2)\mathrm{V}_{\rm obs}(\theta_1, \theta_2)}{\sum_{\theta_2} \mathrm{V}_{\rm obs}(\theta_1, \theta_2)}, \tag{29}$$

(where $\theta_2 = \{\iota, \theta, \phi, \psi\}$ are the parameters being averaged over) as the *volume-weighted fitting factor*. It essentially measures the average of the fractional observable volume loss, weighted by the actual available observable volume, and so simultaneously down-weights the loss in the observable volume for binary configurations to which the detector is relatively less sensitive to begin with. We can give the parameter sets θ_1 and θ_2 different elements than the ones shown here, i.e. $\theta_1 \neq \{m_1, m_2\}$, $\theta_2 \neq \{\iota, \theta, \phi, \psi\}$, $\theta_1 \cup \theta_2 = \{m_1, m_2, \iota, \theta, \phi, \psi\}$, in order to obtain more information about another set of parameters θ'_1.

A. EOBNRv2 templates placed using the TaylorF2 metric

In this section we measure the effectualness of the second-order post-Newtonian hexagonal template bank placement metric described in Ref. [32] when used to place EOBNRv2 waveform templates for aLIGO. The same template placement algorithm was used to place a grid of third-and-a-half-order post-Newtonian order TaylorF2 waveforms for low-mass BBH detection searches for initial LIGO and Virgo observations [18–22]. We construct a template bank which has a desired minimal match of 0.97 for waveforms with component masses between $3M_\odot \leq m_1,\ m_2 \leq 25M_\odot$. This template bank contains 10 753 template grid points in (m_1, m_2) space for the aLIGO noise curve, compared to 373 grid points for the initial LIGO design noise curve. For the template waveforms at each grid point, we use the EOBNRv2 waveforms, rather than TaylorF2 waveforms. Since the metric itself was derived using second-order TaylorF2 waveforms, we do not *a priori* know if this metric is a good measure to use to place template banks for EOBNRv2 waveforms.

To test the effectualness of this template bank, we perform a Monte Carlo simulation over the $3M_\odot \leq m_1, m_2 \leq 25M_\odot$ BBH mass space to find regions where the bank placement algorithm leads to under-coverage. We sample 90 000 points uniformly distributed in individual component masses. For each of these points, we generate an EOBNRv2 waveform for the system with component masses given by the coordinates of the point. We record the $\mathcal{FF}$ of the template bank for each of the randomly generated BBH waveforms in the Monte Carlo simulation. Since we use EOBNRv2 waveforms both to model the true BBH signals and as matched-filter templates, any departure in the fitting factor from unity is due to the placement of the template bank grid.

For a bank of template waveforms constructed with a MM of 0.97, Figs. 1 and 2 show that the $\mathcal{FF}$ of the bank remains above 0.97 for ∼98.5% of all simulated BBH

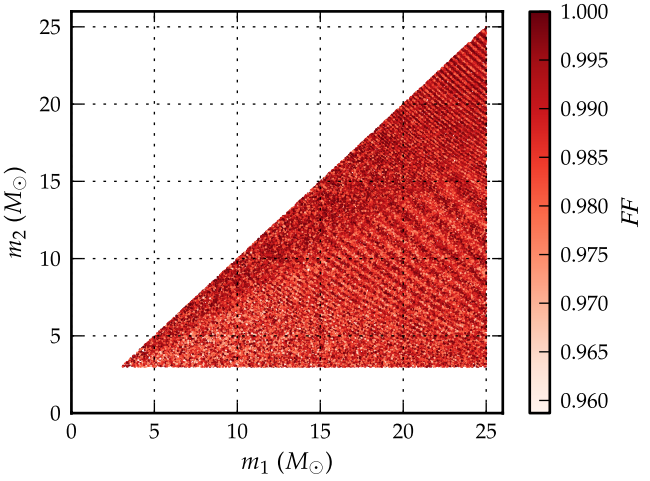

FIG. 1 (color online). This figure shows the effectualness of a bank of EOBNRv2 templates, placed using the 2PN-accurate hexagonal template placement of Ref. [32], to search for a population of BBH signals simulated with EOBNRv2 waveforms. The masses of the BBH population are chosen from a uniform distribution of component masses between 3 and $25M_\odot$. For each injection, we plot the component masses of the injection, and the fitting factor $(\mathcal{FF})$.

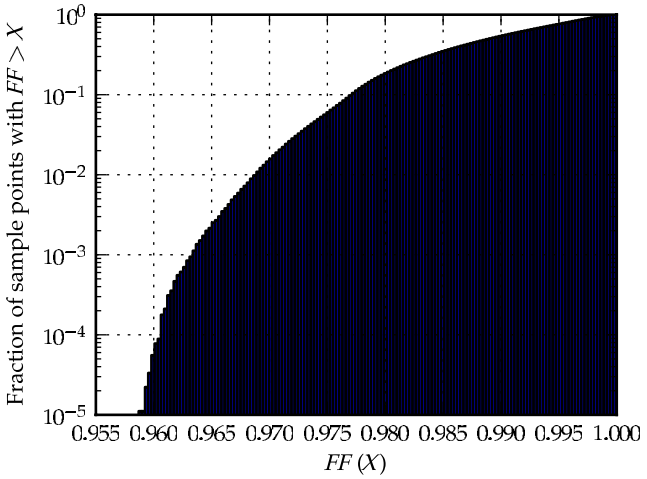

FIG. 2 (color online). This figure shows a cumulative histogram of the fraction of the BBH signal space (on the y axis), where the bank of EOBNRv2 waveforms has an $\mathcal{FF}$ less than the respective values on the x axis. The EOBNRv2 bank has a fitting factor $\mathcal{FF}$ below 0.97 for less than ~1.5% of all simulated signals with component masses m_1, m_2 between $3M_\odot$ and $25M_\odot$.

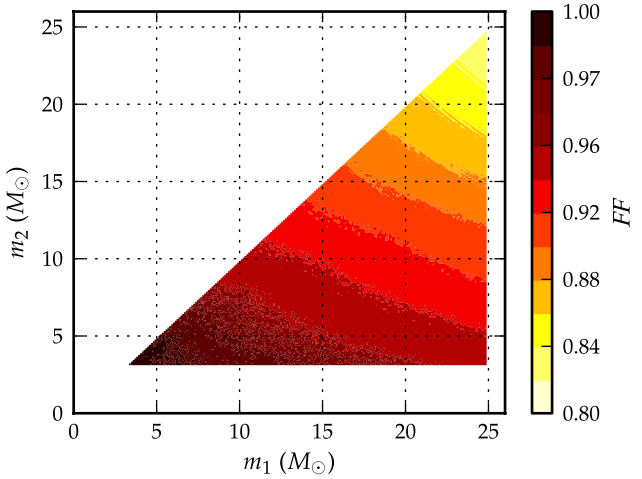

FIG. 3 (color online). The fitting factor $\mathcal{FF}$ of a bank of TaylorF2 waveforms, constructed with MM = 0.97, for a population of BBH systems which are modeled using EOBNRv2 signals.

signals. Less than ~1.5% of signals have a minimal match of less than 0.97, with the smallest value over the 90 000 sampled points being ~0.96. The diagonal features observed in Fig. 1 are due to the hexagonal bank placement algorithm and are related to the ellipses of constant chirp mass in Fig. 4 of Ref. [32]. From these results, we conclude that the existing template bank placement metric adequately covers the BBH mass space with EOBNRv2 waveform templates; it is not necessary to construct a metric specific to the EOBNRv2 model. aLIGO detection searches can employ the second-order post-Newtonian bank placement metric with the hexagonal placement algorithms [30–34] to place template banks for EOBNRv2 waveforms without a significant drop in the recovered signal-to-noise ratio.

B. Effectualness of TaylorF2 templates

We next explore the efficiency of using the computationally cheaper TaylorF2 waveforms to search for a population of BBH signals with component masses between $(3–25)M_\odot$. The signals from this population are modeled with the full EOBNRv2 waveforms. We use the same template bank placement as above; however, now we use the third-and-a-half PN order TaylorF2 model as the template waveforms. This model does not capture the merger and ring-down of BBH signals, as it is terminated at the Schwarzchild test-particle innermost stable circular orbit. Furthermore, it diverges from the true BBH signal in the late inspiral. It is important to determine when these effects become important.

We sample the $(3–25)M_\odot$ BBH component mass space at 100 000 points by generating an EOBNRv2 waveform to generate the "true" signal waveform. We generate a bank of TaylorF2 template waveforms over the same region, and calculate its $\mathcal{FF}$ for each of the sample points against the corresponding EOBNRv2 waveform. Figure 3 shows the distribution of the $\mathcal{FF}$ obtained for the TaylorF2 bank. Clearly the TaylorF2 bank is not effectual for the entire BBH region considered, with mismatches of up to 18% observed. We divide the sampled component mass space into subregions which consist of systems with total masses below different thresholds, and compute the minimal fitting factor of the bank over those. In Fig. 4, the blue (solid)

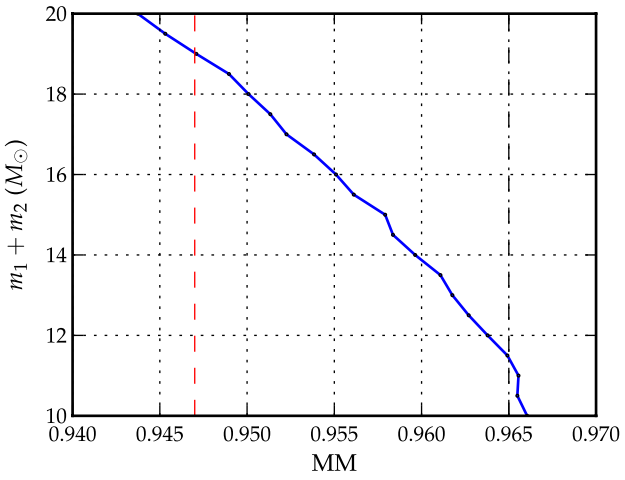

FIG. 4 (color online). The (blue) curve shows the upper bound on the total mass for the subregion over which the TaylorF2 bank has a minimal fitting factor as given on the x axis. We observe that the TaylorF2 bank has a minimal fitting factor of 0.965 (0.947) for the region with total masses below $\sim 11.4M_\odot(19M_\odot)$. The minimal fitting factor is the fitting-factor value which is less than the fitting factors of the TaylorF2 bank for $\geq$ 99.75% of the points sampled in the subregion.

curve shows the upper limit on total mass for different subregions against the minimal fitting factor of the TaylorF2 bank over those. The minimal fitting factor over a subregion is taken to be the fitting-factor value that is less than the fitting factors for $\geq 99.75\%$ of the points sampled in the subregion. We find that the TaylorF2 template bank has an $\mathcal{FF}$ above 0.965 (0.947) for the region with total masses below $11.4M_\odot$ ($19M_\odot$). We conclude that the TaylorF2 bank is effectual for BBH signals below $\sim 11.4M_\odot$.

The value of our limit on total mass is in agreement with the previous study in Ref. [45]; however, this analysis used the EOBNRv1 model [70] and an older version of the Advanced LIGO noise curve [45]. This agreement provides confidence that this limit will be robust in aLIGO searches and we propose this limit as the upper cutoff for the computationally cheaper TaylorF2 search. To investigate the loss in the $\mathcal{FF}$ due to the mismatch in the template and signal waveform models, we also performed a Monte Carlo simulation using a denser TaylorF2 bank with MM = 0.99. We found that by using this dense bank of third-and-a-half-order TaylorF2 waveforms we can relax the limit on the upper mass to $\sim 16.3M_\odot$ ($21.8M_\odot$) and still achieve an $\mathcal{FF}$ above 0.965 (0.947) for over 99.75% of the signals sampled in the region. However, increasing the minimal match increases the size of the template bank from 10 753 to 29 588 templates. This is a significant increase, compared to the cost of filtering with EOBNRv2 templates.

C. Effect of subdominant modes

Having established that the second-order post-Newtonian hexagonal template bank is effectual for placing a bank of EOBNRv2 templates, we now investigate the effect of neglecting subdominant modes in BBH searches. The sensitivity reach of the aLIGO detectors is normally computed assuming that the search is only sensitive to the dominant $l = m = 2$ mode of the gravitational waveform. For binary black hole signals, subdominant modes may contain significant power [47]. A search that includes these modes could, in principle, have an increased reach (and hence event rate) compared to a search that only uses the dominant mode. The EOBNRv2 model of Ref. [15] has been calibrated against higher-order modes from numerical relativity simulations. We investigate the effect of ignoring these modes in a search by modeling the BBH signal as an EOBNRv2 signal containing the dominant and subdominant multipoles, $h_{lm} = h_{22}, h_{21}, h_{33}, h_{44}, h_{55}$ (which we call EOBNRv2HM) and computing the fitting factor of leading-order EOBNRv2 templates placed using the TaylorF2 metric.

We simulate a population of BBH signals by sampling 100 000 systems uniformly in the $m_1, m_2 \in [3, 25]M_\odot$ component-mass space. These EOBNRv2HM signals are uniformly distributed in sky-location angles and inclination and polarization angles, which appear in the detector's response function to the gravitational-wave signal [71]. The template bank is again placed with a desired minimal match of 0.97 and for each of the signal waveforms, we calculate the $\mathcal{FF}$ against the entire bank of EOBNRv2 waveform templates. Figure 5 (left panel) shows the value of the $\mathcal{FF}$ of the bank of EOBNRv2 waveform templates over the sampled component-mass space. As expected, the highest fitting factors are observed close to the equal mass line, since when the mass ratio is close to unity, the amplitude of the subleading waveform modes is several orders of magnitude smaller than the amplitude of the

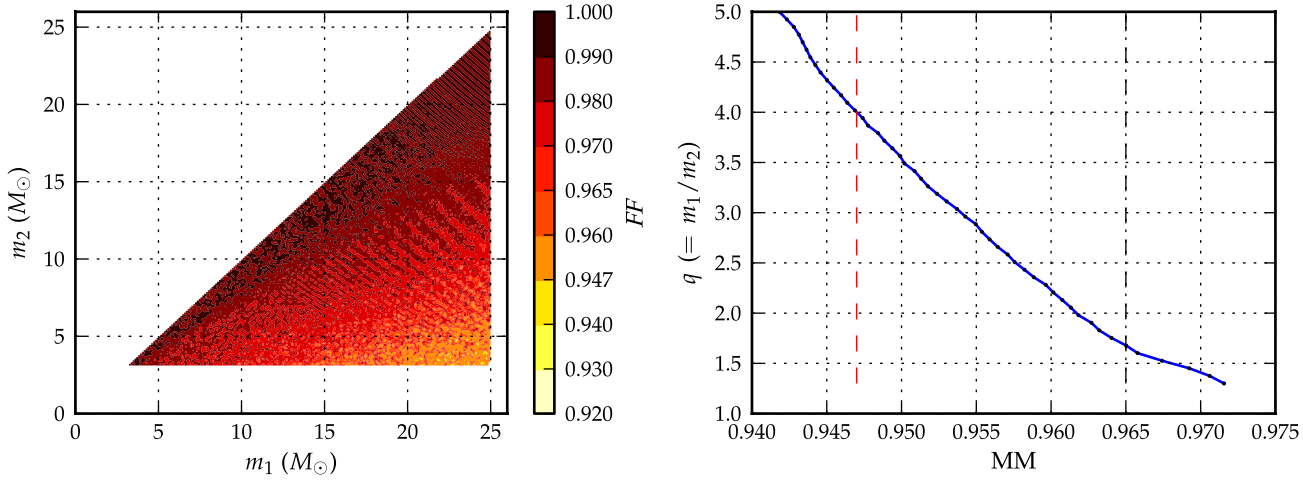

FIG. 5 (color online). (left) The $\mathcal{FF}$ of a bank of EOBNRv2 waveforms, constructed with a minimal match of 0.97 at each point in the stellar-mass BBH component-mass region. While the templates are modeled as the dominant mode $l = m = 2$ EOBNRv2 waveforms, the signals are modeled including the subdominant waveform modes as well (EOBNRv2HM). (right) This figure shows the upper bound on the mass ratio (q) for the region where a bank of EOBNRv2 templates has a minimal fitting factor as given on the x axis. We observe that for the region with $q \leq 1.68(4)$, the minimum match of the bank is below 0.965 (0.947). From both figures, we notice a systematic fall in the coverage of the EOBNRv2 template bank with increasing mass ratio.

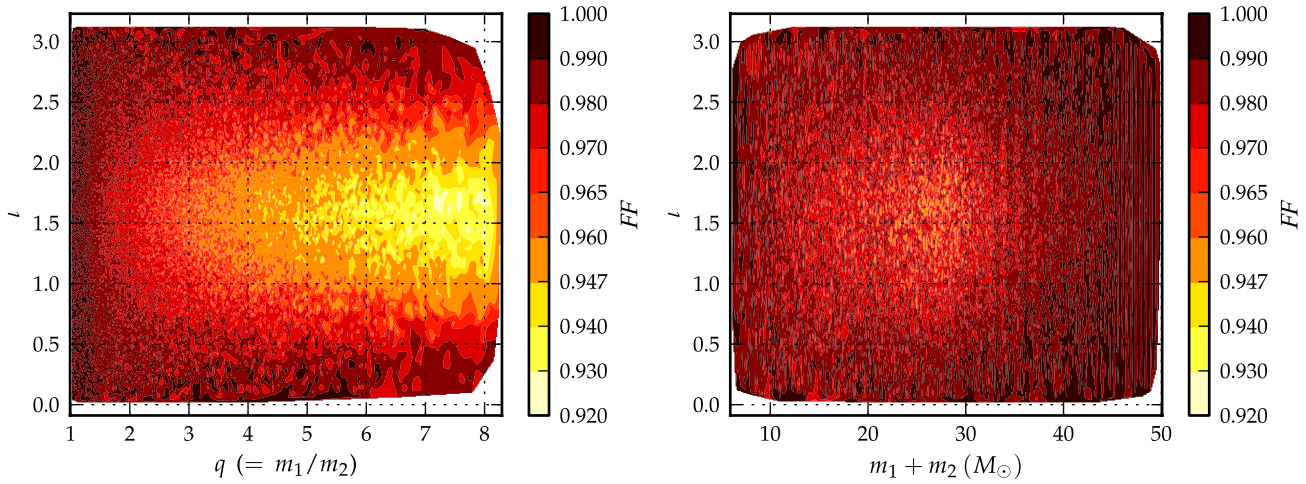

FIG. 6 (color online). (left) The $\mathcal{FF}$ of a bank of EOBNRv2 waveforms, constructed with a minimal match of 0.97 at each point in the stellar-mass BBH $q - \iota$ space. While the templates are modeled as the dominant mode $l = m = 2$ EOBNRv2 waveforms, the signals are modeled including the subdominant waveform modes as well (EOBNRv2HM). We observe a loss in fitting factors—up to ~8%—for systems with high mass ratios (q) *and* inclination angle (ι) close to $\pi/2$. (right) The $\mathcal{FF}$ for the same population of signals, now shown on the $M - \iota$ plane. We observe the loss in fitting factors to be relatively less for more massive binaries.

dominant mode. As the mass ratio increases, the relative amplitude of the subleading multipoles increases, as illustrated by Fig. 1 of Ref. [15] and the fitting factor decreases. This pattern is brought out further in Fig. 6 (left panel), where we show the $\mathcal{FF}$ values in the mass ratio – inclination angle ($q - \iota$) plane. We observe that when the orbital angular momentum is either parallel or antiparallel to the line of sight from the detector, the subleading multipoles do not contribute significantly to the signal. This is what we would expect from Eq. (13), as the spin-weighted harmonics are proportional to $\sin(\frac{\iota}{2})\cos(\frac{\iota}{2})$, except when $l = m = 2$. Similar to Sec. III B, we divide the sampled component-mass space into subregions bounded by $1 \leq q \leq q_{\rm threshold}$, and compute the minimal fitting factor of the EOBNRv2 template bank over those. In Fig. 5 (right panel), the blue (solid) curve shows the value of $q_{\rm threshold}$ for each restricted subregion against the minimal fitting factor of the bank over the same. For systems with mass ratio q below 1.68 (4), we find that the $\mathcal{FF}$ of the EOBNRv2 waveform bank is above 0.965 (0.947) over

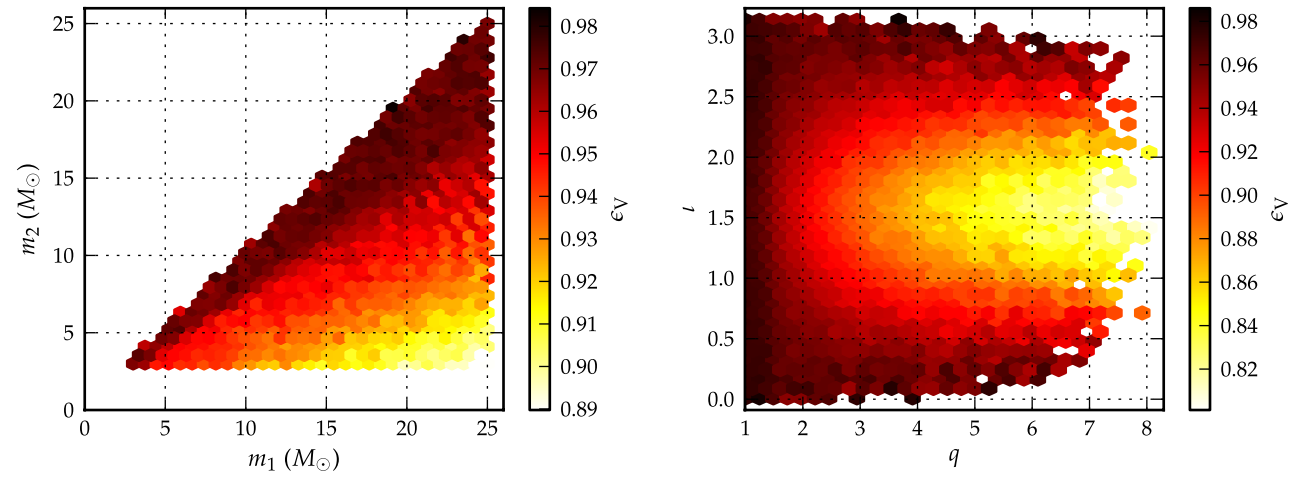

FIG. 7 (color online). (left) This figure shows $\epsilon_{\rm V}(\theta_1 = \{m_1, m_2\})$ in the component-mass space [see Eq. (29)]. This gives the fraction of the total observable volume that is visible to a search which uses the leading order $l = m = 2$ EOBNRv2 waveform template bank, placed with the 2PN-accurate TaylorF2 bank placement metric. For a population of signals that is distributed uniformly in spacial volume, this is equivalent to the fraction of the maximum possible event observation rate that we get with the use of a discrete bank of matched filters. We observe that the loss in event observation rate, averaged over all parameters (uniformly distributed) but $\theta_1 = \{m_1, m_2\}$, does not exceed ~11% for any region of the component-mass space. (right) This figure shows $\epsilon_{\rm V}(\theta_1 = \{q, \iota\})$ over the $q - \iota$ plane. We note that the maximum averaged loss in the detection rate is for systems with high mass ratios *and* $\iota \in [1.08, 2.02]$, and can go as high as ~20% for such systems.

99.75% of this restricted region. These results demonstrate that the effect of ignoring subdominant modes does not cause a significant loss in the total possible signal-to-noise ratio if the mass ratio is less than 1.68. A similar analysis over the range of possible inclination angles shows that the EOBNRv2 waveform bank has fitting factors above 0.965 (0.947) for systems with $2.68(2.02) \leq \iota \leq \pi$, and $0 \leq \iota \leq 0.31(1.08)$ (see Fig. 6, left panel).

Fitting factors as low as 0.92 are observed for systems with high mass ratios *and* inclination angle close to $\pi/2$. As these are also binary configurations to which the detector is relatively less sensitive [47], fitting factors alone do not answer the question of where in the parameter space we lose the most in terms of the detection rate. To address this question, we compute the volume-weighted fitting factors ϵ_{V} of the EOBNRv2 template bank, over the sampled BBH parameter space. This gives us an estimate of the expected loss in the detection rate if the source population is distributed uniformly in spacial volume and uniformly in intrinsic and extrinsic source parameters. Figure 7 (left panel) shows ϵ_{V} calculated in bins over the component-mass space. In this figure, the color of each bin in the component-mass plane corresponds to—for a population that has all other parameters, i.e., the inclination angle and sky/polarization angles uniformly distributed over their possible ranges—the averaged loss in the detection rate incurred due to the use of a bank of leading-order $l = m = 2$ EOBNRv2 templates, placed using the 2PN bank placement metric. We observe that the maximum loss incurred goes up to only ~10%–11%, which is within our acceptable threshold. Looking at Fig. 6 (left panel), the maximum loss in the fitting factor occurs for systems with inclination angles close to $\pi/2$, but (for the same mass ratio) these get averaged out with systems with inclinations close to 0 or π, which leads to the low averaged detection-rate losses we observe in Fig. 7 (left panel). The right panel of Fig. 7 shows the same quantity, ϵ_{V}, calculated over bins in the mass ratio–inclination angle plane. As expected, we observe that, letting all other parameters be distributed uniformly over their possible ranges, systems with high mass ratios *and* inclination angles close to $\pi/2$ will incur (averaged) losses in observation volume of up to ~20%.

These results suggest that a search that includes higher-order modes could achieve a nontrivial increase in sensitivity over leading-order mode templates, only in detecting systems with high q *and* $1.08 \leq \iota \leq 2.02$. However, an algorithm that includes subdominant modes could have an increased false-alarm rate (background) over a search that includes only the leading-order mode, and hence the overall gain in search efficiency might not be significant.

IV. CONCLUSIONS

We used the TaylorF2 second-order post-Newtonian hexagonal placement algorithm of Refs. [32–34] to construct a template bank of EOBNRv2 waveforms with MM of 0.97. We calculated the fitting factor ($\mathcal{FF}$) of this bank against ~90000 simulated EOBNRv2 signals with component masses uniformly distributed between $3M_{\odot} \leq m_1, m_2 \leq 25M_{\odot}$. We find that the $\mathcal{FF}$ of the template bank is greater than 0.97 for 98.5% of the simulated EOBNRv2 signals, assuming the zero-detuning high-power noise spectrum for aLIGO sensitivity [35]. We conclude that the existing placement algorithm is effectual for use in aLIGO BBH searches, assuming that EOBNRv2 is an accurate model of BBH signals in this mass region. We then demonstrated that the use of the computationally cheaper third-and-a-half-order TaylorF2 waveform results in a loss in search efficiency due to inaccuracies of the post-Newtonian approximation, and the neglect of merger-ring-down for BBHs with a total mass $M > 11.4M_{\odot}$. However, below this limit the TaylorF2 model is an acceptable signal for BBH searches. This was done using a bank with a MM of 0.97. By increasing the density of the bank to 0.99 MM, the limit on the total mass can be relaxed to $16.3M_{\odot}$, with an increase in computational cost due to the number of templates increasing by a factor of ~2.7. Finally, we investigated the loss in the SNR incurred by using template banks constructed using only the leading-order mode of EOBNRv2 waveforms. We found that a leading-order $l = m = 2$ EOBNRv2 template bank constructed with a MM of 0.97 is effectual to search for BBHs for which $1 \leq (m_1/m_2) \leq 1.68$ or $\iota \geq 2.68$ or $\iota \leq 0.31$ radians, and there is no significant loss in the potential signal-to-noise ratio for systems with q as high as 4 or $2.02 \leq \iota \leq 2.68$ or $0.31 \leq \iota \leq 1.08$. We also observed that the maximum loss in the detection rate for a binary with given mass parameters—averaging over other parameters, which are taken to be uniformly distributed over their possible ranges—goes only to a maximum of ~10%–11%. For any given pair of binary masses, the loss is highest when the binary is inclined at $\simeq \pi/2$, and can go up to ~20%, and is lower when its angular momentum is close to being parallel or antiparallel to the line of sight from the detector. These effects average out, and hence for a population that is expected to have a uniform distribution of inclination angles (and uniform distribution in spacial volume), the average loss in the detection rate was estimated to be not higher than ~11%. Thus, using EOBNRv2HM templates is unlikely to give a significant increase in the range to which such a population of sources can be detected. For BBHs with $(m_1/m_2) \geq 4$ *and* $1.08 \leq \iota \leq 2.02$, detection searches could possibly gain sensitivity by the use of EOBNRv2HM waveforms if they can be implemented without increasing the false-alarm rate.

Our results suggest that a significant portion of the nonspinning stellar-mass BBH parameter space can be searched for using LIGO's existing search algorithms. For systems with a total mass below $\sim 11.4M_{\odot}$ template banks of TaylorF2 can be used without a significant loss in the event rate. For higher-mass systems, neglecting

high-order modes in an EOBNRv2 search does not cause a substantial reduction in the maximum possible reach of BBH searches. Finally, we note that our study does not consider BBH systems with BH masses higher than $M = 25M_{\odot}$, or the effect of black hole component spins. Future work will extend this study for systems with spinning and/or precessing black holes and consider the effect of non-Gaussian transients in real detector noise.

ACKNOWLEDGMENTS

We are grateful to Stefan Ballmer, Jolien Creighton, Ian Harry, Eliu Huerta, Peter Saulson, and Matt West for helpful comments. We thank Tom Dent for carefully reading this manuscript and Yi Pan for fixing a problem with the EOBNRv2 model discovered during this work. We are grateful to Evan Ochsner and Craig Robinson for writing the LAL implementation of EOBNRv2 against which our code was validated. We are also grateful to the anonymous peer-review referee for their constructive comments. This work was supported by NSF Grants No. PHY-0847611 and No. PHY-0854812, and a Research Corporation for Science Advancement Cottrell Scholar award. Computations were carried out on the SUGAR cluster which is supported by NSF Grants No. PHY-1040231, No. PHY-1104371, and No. PHY-0600953, and by Syracuse University ITS. Part of this work was carried out at the Kavli Institute for Theoretical Physics at Santa Barbara University, supported in part by NSF Grant No. PHY-0551164.

[1] G. M. Harry *et al.* (LIGO Scientific Collaboration), Classical Quantum Gravity **27**, 084006 (2010).
[2] F. Acernese *et al.* (The Virgo Collaboration), Virgo Technical Document, Report No. VIR-0027A-09.
[3] K. Somiya (KAGRA Collaboration), Classical Quantum Gravity **29**, 124007 (2012).
[4] S. Waldman (the LIGO Scientific Collaboration), arXiv:1103.2728.
[5] S. W. Hawking and W. Israel, *Three Hundred Years of Gravitation* (Cambridge University Press, Cambridge, England, 1987).
[6] J. Abadie *et al.* (LIGO Scientific Collaboration, Virgo Collaboration), Classical Quantum Gravity **27**, 173001 (2010).
[7] A. Buonanno and T. Damour, Phys. Rev. D **59**, 084006 (1999).
[8] T. Damour, A. Nagar, M. Hannam, S. Husa, and B. Brugmann, Phys. Rev. D **78**, 044039 (2008).
[9] A. Buonanno, Y. Pan, H. P. Pfeiffer, M. A. Scheel, L. T. Buchman, and L. E. Kidder, Phys. Rev. D **79**, 124028 (2009).
[10] T. Damour and A. Nagar, Phys. Rev. D **79**, 081503 (2009).
[11] T. Damour and A. Nagar, Phys. Rev. D **77**, 024043 (2008).
[12] T. Damour, A. Nagar, E. N. Dorband, D. Pollney, and L. Rezzolla, Phys. Rev. D **77**, 084017 (2008).
[13] A. Buonanno and T. Damour, Phys. Rev. D **62**, 064015 (2000).
[14] T. Damour, B. R. Iyer, P. Jaranowski, and B. S. Sathyaprakash, Phys. Rev. D **67**, 064028 (2003).
[15] Y. Pan, A. Buonanno, M. Boyle, L. T. Buchman, L. E. Kidder, H. P. Pfeiffer, and M. A. Scheel, Phys. Rev. D **84**, 124052 (2011).
[16] E. Berti, V. Cardoso, and C. M. Will, Phys. Rev. D **73**, 064030 (2006).
[17] Y. Mino, M. Sasaki, M. Shibata, H. Tagoshi, and T. Tanaka, Prog. Theor. Phys. Suppl. **128**, 1 (1997).
[18] J. Abadie *et al.* (LIGO Scientific Collaboration, Virgo Collaboration), Phys. Rev. D **85**, 082002 (2012).
[19] J. Abadie *et al.* (LIGO Scientific Collaboration, Virgo Collaboration), Phys. Rev. D **82**, 102001 (2010).
[20] B. Abbott *et al.* (LIGO Scientific Collaboration), Phys. Rev. D **80**, 047101 (2009).
[21] B. Abbott *et al.* (LIGO Scientific Collaboration), Phys. Rev. D **79**, 122001 (2009).
[22] E. Messaritaki (LIGO Scientific Collaboration), Classical Quantum Gravity **22**, S1119 (2005).
[23] L. A. Wainstein and V. D. Zubakov, *Extraction of signals from noise* (Prentice-Hall, Englewood Cliffs, NJ, 1962).
[24] B. Allen, W. G. Anderson, P. R. Brady, D. A. Brown, and J. D. E. Creighton, Phys. Rev. D **85**, 122006 (2012).
[25] F. Ozel, D. Psaltis, R. Narayan, and J. E. McClintock, Astrophys. J. **725**, 1918 (2010).
[26] B. S. Sathyaprakash and S. V. Dhurandhar, Phys. Rev. D **44**, 3819 (1991).
[27] R. Balasubramanian, B. S. Sathyaprakash, and S. V. Dhurandhar, Phys. Rev. D **53**, 3033 (1996).
[28] T. A. Apostolatos, Phys. Rev. D **52**, 605 (1995).
[29] K. Cannon, A. Chapman, C. Hanna, D. Keppel, A. C. Searle, and A. J. Weinstein, Phys. Rev. D **82**, 044025 (2010).
[30] B. J. Owen, Phys. Rev. D **53**, 6749 (1996).
[31] B. S. Sathyaprakash, Phys. Rev. D **50**, R7111 (1994).
[32] S. Babak, R. Balasubramanian, D. Churches, T. Cokelaer, and B. Sathyaprakash, Classical Quantum Gravity **23**, 5477 (2006).
[33] B. J. Owen and B. S. Sathyaprakash, Phys. Rev. D **60**, 022002 (1999).
[34] T. Cokelaer, Phys. Rev. D **76**, 102004 (2007).
[35] D. Shoemaker (LIGO Collaboration), "*Advanced LIGO anticipated sensitivity curves*," LIGO Document Report No. T0900288-v3, 2009.
[36] C. Cutler and E. E. Flanagan, Phys. Rev. D **49**, 2658 (1994).
[37] S. Droz, D. J. Knapp, E. Poisson, and B. J. Owen, Phys. Rev. D **59**, 124016 (1999).
[38] L. Blanchet, T. Damour, G. Esposito-Farese, and B. R. Iyer, Phys. Rev. Lett. **93**, 091101 (2004).

[39] L. Blanchet and B. R. Iyer, Phys. Rev. D **71**, 024004 (2005).
[40] P. Jaranowski and G. Schaefer, Ann. Phys. (Berlin) **9**, 378 (2000).
[41] P. Jaranowski and G. Schafer, Phys. Rev. D **60**, 124003 (1999).
[42] T. Damour, P. Jaranowski, and G. Schaefer, Phys. Lett. B **513**, 147 (2001).
[43] L. E. Kidder, Phys. Rev. D **77**, 044016 (2008).
[44] L. Blanchet, G. Faye, B. R. Iyer, and S. Sinha, Classical Quantum Gravity **25**, 165003 (2008).
[45] A. Buonanno, B. R. Iyer, E. Ochsner, Y. Pan, and B. S. Sathyaprakash, Phys. Rev. D **80**, 084043 (2009).
[46] D. McKechan, Ph.D. thesis, 2011, arXiv:1102.1749.
[47] L. Pekowsky, J. Healy, D. Shoemaker, and P. Laguna, arXiv:1210.1891.
[48] L. Blanchet, Living Rev. Relativity **9**, 4 (2006).
[49] F. Pretorius, Phys. Rev. Lett. **95**, 121101 (2005).
[50] F. Pretorius, Classical Quantum Gravity **23**, S529 (2006).
[51] M. A. Scheel, M. Boyle, T. Chu, L. E. Kidder, K. D. Matthews, and H. P. Pfeiffer, Phys. Rev. D **79**, 024003 (2009).
[52] J. A. Gonzalez, U. Sperhake, and B. Brugmann, Phys. Rev. D **79**, 124006 (2009).
[53] D. Pollney, C. Reisswig, E. Schnetter, N. Dorband, and P. Diener, Phys. Rev. D **83**, 044045 (2011).
[54] C. O. Lousto, H. Nakano, Y. Zlochower, and M. Campanelli, Phys. Rev. Lett. **104**, 211101 (2010).
[55] L. T. Buchman, H. P. Pfeiffer, M. A. Scheel, and B. Szilagyi, Phys. Rev. D **86**, 084033 (2012).
[56] P. Ajith *et al.*, Classical Quantum Gravity **29**, 124001 (2012).
[57] T. Damour, P. Jaranowski, and G. Schafer, Phys. Rev. D **62**, 084011 (2000).
[58] T. Damour, B. R. Iyer, and A. Nagar, Phys. Rev. D **79**, 064004 (2009).
[59] A. Buonanno and T. Damour, Phys. Rev. D **59**, 084006 (1999).
[60] A. Buonanno, Y. Chen, and T. Damour, Phys. Rev. D **74**, 104005 (2006).
[61] "LSC Algorithm Library," https://www.lsc-group.phys.uwm.edu/daswg/projects/lalsuite.html.
[62] J. Mathews and R. L. Walker, *Mathematical Methods of Physics* (W. A. Benjamin, San Francisco, 1970), 2nd ed.
[63] L. Blanchet, T. Damour, B. R. Iyer, C. M. Will, and A. G. Wiseman, Phys. Rev. Lett. **74**, 3515 (1995).
[64] L. Blanchet, G. Faye, B. R. Iyer, and B. Joguet, Phys. Rev. D **65**, 061501 (2002).
[65] L. Blanchet, T. Damour, G. Esposito-Farese, and B. R. Iyer, Phys. Rev. Lett. **93**, 091101 (2004).
[66] E. Poisson and C. M. Will, Phys. Rev. D **52**, 848 (1995).
[67] L. Lindblom, B. J. Owen, and D. A. Brown, Phys. Rev. D **78**, 124020 (2008).
[68] L. Lindblom, J. G. Baker, and B. J. Owen, Phys. Rev. D **82**, 084020 (2010).
[69] L. S. Finn and D. F. Chernoff, Phys. Rev. D **47**, 2198 (1993).
[70] A. Buonanno, Y. Pan, J. G. Baker, J. Centrella, B. J. Kelly, S. T. McWilliams, and J. R. van Meter, Phys. Rev. D **76**, 104049 (2007).
[71] B. Sathyaprakash and B. Schutz, Living Rev. Relativity **12**, 2 (2009).